A Biomimetic steering robot for Minimally invasive surgery application

Gang Chen, Minh Tu Pham, Talel Maalej, Hassen Fourati, Richard Moreau, Sylvie Sesmat

A Biomimetic steering robot for Minimally invasive surgery application

G. Chen [a,*]

[a] *Unilever R&D, Port Sunlight, United Kingdom*

M.T. Pham, T. Maalej, H. Fourati, R. Moreau, S. Sesmat [b]

[b] *Laboratoire Ampère, UMR CNRS 5005, INSA-Lyon, Université de Lyon, F-69621, France*

Abstract

Minimally Invasive Surgery represents the future of many types of medical interventions such as keyhole neurosurgey or transluminal endoscopic surgery. These procedures involve insertion of surgical instruments such as needles and endoscopes into human body through small incision/ body cavity for biopsy and drug delivery. However, nearly all surgical instruments for these procedures are inserted manually and there is a long learning curve for surgeons to use them properly. Many research efforts have been made to design active instruments (endoscope, needles) to improve this procedure during last decades. New robot mechanisms have been designed and used to improve the dexterity of current endoscope. Usually these robots are flexible and can pass the constrained space for fine manipulations. In recent years, a continuum robotic mechanism has been investigated and designed for medical surgery. Those robots are characterized by the fact that their mechanical components do not have rigid links and discrete joints in contrast with traditional robot manipulators. The design of these robots is inspired by movements of natural animals such as tongues, elephant trunks and tentacles. The unusual compliance and redundant degrees of freedom of these robots provide strong potential to achieve delicate tasks successfully even in cluttered and unstructured environments.

This chapter will present a complete application of a continuum robot for Minimally Invasive Surgery of colonoscopy. This system is composed of a micro-robotic tip, a set of position sensors and a real-time control system for guiding the exploration of colon. Details will be described on the modeling of the used pneumatic actuators, the design of the mechanical component, the kinematic model analysis and the control strategy for automatically guiding the progression of the device inside the human colon. Experimental results will be presented to check the performances of the whole system within a transparent tube.

Preprint submitted to IN-TECH *9 September 2009*

1 Introduction

Robotics has increasingly become accepted in the past 20 years as a viable solution to many applications in surgery, particularly in the field of Minimally Invasive Surgery (MIS)[1]. Minimally Invasive Surgery represents the future of many types of medical interventions such as keyhole neurosurgey or transluminal endoscopic surgery. These procedures involve insertion of surgical instruments such as needles and endoscopes into human body through small incision/ body cavity for biopsy and drug delivery. However, nearly all surgical instruments for these procedures are inserted manually and they are lack of dexterity in small constrained spaces. As a consequence, there is a long learning curve for surgeons to use them properly. Many research efforts have been made to improve the functionalities of current instruments by designing active instruments (endoscope, needles) using robotic mechanisms during the last decades, such as snake robot for throat surgery [2] or active cannula [3]. Studies are currently underway to evaluate the value of these new devices. Usually these robots are micro size and very flexible so that they can pass the constrained space for fine manipulations. Furthermore, how to steer these robots into targets safely during the insertion usually needs additional sensors, such as MRI imaging and US imaging, and path planning algorithms are also needed to be developped for the intervention.

Colonoscopy is a typical MIS procedure that needs the insertation of long endoscope inside the human colon for diagnostics and therapy of the lower gastrointestinal tract including the colon. The difficulty of the insertion of colonoscope into the human colon and the pain of the intervention brought to the patient hinders the diagnostics of colon cancer massively. This chapter will present a novel steerable robot and guidance control strategy for colonoscopy interventions which reduces the challenge associated with reaching the target.

1.1 Colonoscopy

Today, colon cancer is an increasing medical concern in the world, where the second frequent malignant tumor is found in industrialized countries [4]. There are several different solutions to detect this kind of cancer, but only colonoscopy can not only make diagnostics, but make therapy. Colonoscopy is a procedure which is characterized by insertion of endoscopes into the human colon for inspection of the lower gastrointestinal tract including the colon in order to stop or to slow the progression of the illness. The anatomy of the

* Corresponding author.
Email address: gang.chen@unilever.com (G. Chen).

colon is showed in Fig. 1.

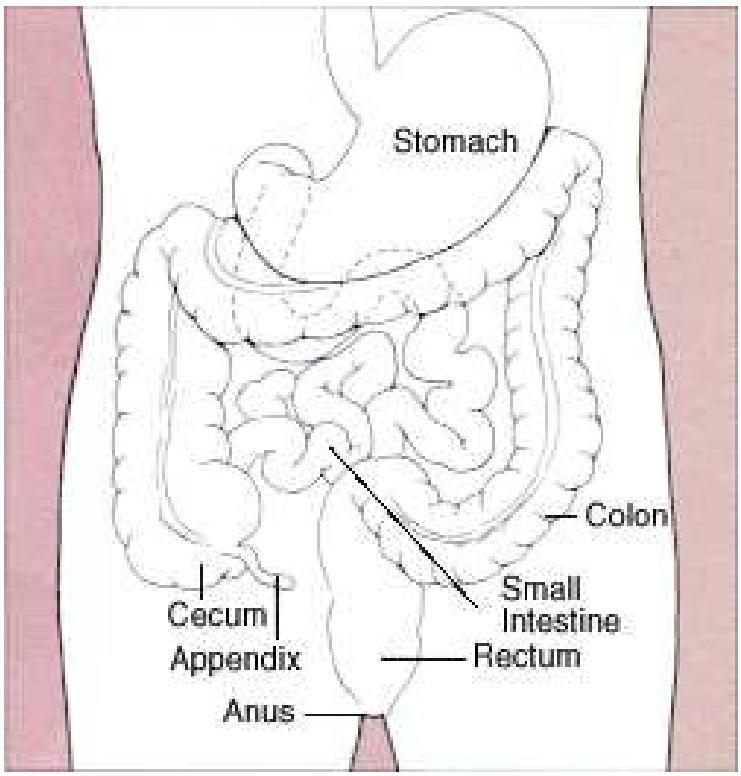

Fig. 1. The anatomy of the colon

The instrument used for diagnostics and operation of the human colon is called endoscope (also colonoscope) which is about 1.5cm in diameter and from 1.6 to 2 meters in length. Colonoscopy is one of the most technically demanding endoscopic examinations and tends to be very unpopular with patients because of many sharp bends and constrained workspace. The main reason lies in the characteristics of current colonoscopes, which are quite rigid and require the doctor to perform difficult manoeuvres for long insertion with minimal damage of the colon wall [5,6].

1.2 State of the art: Robotic colonoscopy

Since the human colon is a tortuous "tube" with several sharp bends, the insertion of the colonoscope requires the doctor to exert forces and rotations at shaft outside of the patient, thus causing discomfort to the patient. The complexity of the procedure for doctors and the discomfort experienced by the patient of current colonoscopies lead many researchers to choose the automated colonoscopy method. In [7], the authors proposed the concept of

automated colonoscopy (also called robotic colonoscopy) from two aspects: locomotion and steering of the distal end, which are the two main actions during a colonoscopy. In order to facilitate the operation of colonoscopy, some studies on the robotic colonoscopy have been carried out from these two aspects. Most current research on autonomous colonoscopies have been focused on the self-propelled robots which utilize various locomotion mechanisms [8–13]. Among them, inchworm-like locomotion attracted much more attention [9,10]. However, most of the current inchworm-based robotic systems [9–12] showed low efficiency of locomotion for exploring the colon because of the structure of the colon wall: slippery and different diameters at each section.
Another aspect work that could improve the performance of current colonoscopies is to design an autonomous steering robot for guidance inside the colon during the colonoscopy. Fukuda *et al.* [6] proposed Shape Memory Alloy (SMA) based bending devices, called as Micro-Active Catheter (MAC), with two degrees of freedom. With three MACs connected together in series, an angle of bend of nearly 80° is possible. In [11], a bendable tip has been also designed and fabricated by using a silicone bellows with a length of 30mm. It contains three small SMA springs with a 120° layout. This device allows a 90^o bending in three directions. These flexible steering tips are are only parts of the whole self-propelling robots, however those works did not focus on how to control this special robot to endow it with a capability for autonomous guidance [11,12,14,15].
Since 2001, there is another method to perform colon diagnostics: capsule endoscopy [16,17]. With a camera, a light source, a transmitter and power supply integrated into a capsule, the patient can swallow and repel it through natural peristalsis without any pain. Although capsule endoscopy has the advantage in contrast with current endoscopy, capsule endoscopy can't be used to perform the diagnostics more thoroughly and actively. Recently, different active locomotion mechanisms have been investigated and designed to address this problem, such as clamping mechanism [18], SMA-based [19,20], magnet-based [21] locomotion and biomimetic gecko[22] .

1.3 An approach to steering robot for colonoscopy

The objective of our work in this chapter is different from all the works from other laboratories, which is to design a robot with high dexterity capable of guiding the progression with minimal hurt to the colon wall. Our approach emphasizes a robotic tip with a novel design mounted on the end of the traditional colonoscope or similar instruments.
The whole system for semi-autonomous colonoscopy will be presented in this chapter. It is composed of a microtip, which is based on a continuum robot mechanism, a proximity multi-sensor system and high level real-time control

system for guidance control of this robot. The schema of the whole system, called Colobot, is shown in Fig. 2. Section 2 briefly presents the Colobot and its proximity sensor system. Then section 3 will present model analysis of Colobot system and the validation of kinematic model in section 4. In section 5 guidance control strategy is presented and control architecture and implementation will be described in Section 5.2. Finally, experimental results in a colon-like tube will be presented to verify the performance of this semi-autonomous system.

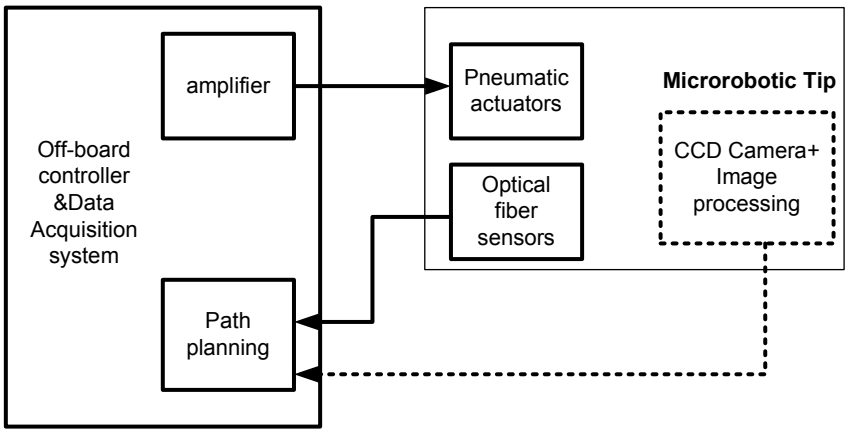

Fig. 2. The scheme of the whole system

2 Micro-robotic tip: Colobot

Biologically-inspired continuum robots [23] have attracted much interest from robotics researchers during the last decades to improve the capability of manipulation in constrained space. These kinds of systems are characterized by the fact that their mechanical components do not have rigid links and discrete joints in contrast with traditional industry robots. The design of these robots are inspired by movements of natural animals such as tongues, elephant trunks and tentacles etc. The unusual compliance and redundant degrees of freedom of these robots provide strong potential to achieve delicate tasks successfully even in cluttered and/or unstructured environments such as undersea operations [24], urban search and rescue, wasted materials handling [25], Minimally Invasive Surgery [2,10,14,26].
The Colobot [27] designed for our work, is a small-scaled continuum robot. Due to the size requirement of the robot, there are challenges on how to miniaturize sensor system integrated into the small-scale robot to implement automatic guidance of progression inside the human colon. This section will present the detailed design of the Colobot and its fibre-optic proximity sensor system.

2.1 Colobot

The difference between our robotic tip and other existing continuum robots is the size. Our design is inspired by pioneer work [28] on a flexible micro-actuator (FMA) based on silicone rubber. Fig. 3(a) shows our design of the Colobot. The robotic tip has 3 DOF (Degree of Freedom), which is a unique

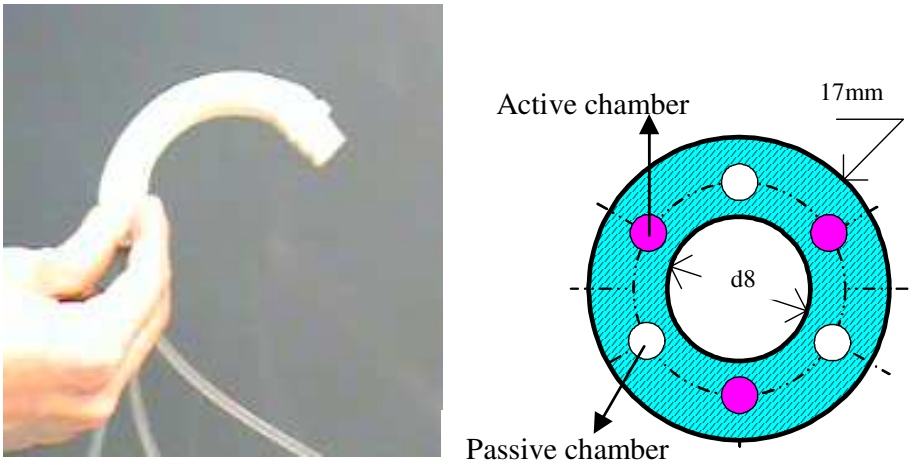

(a) Colobot (b) Cross section of Colobot

Fig. 3. Colobot and its cross section

unit with 3 active pneumatic chambers regularly disposed at 120 degrees apart. These three chambers are used for actuation; three other chambers shown in fig. 3(b) are designed to optimize the mechanical structure in order to reduce the radial expansion of active chambers under pressure. The outer diameter of the tip is 17 mm that is lesser than the average diameter of the colon. The diameter of the inner hole is 8mm, which is used in order to place the camera or other lighting tools. The weight of the prototype is 20 grams. The internal pressure of each chamber is independently controlled by using pneumatic jet-pipe servovalves. The promising result obtained from the preliminary experiment showed that this tip could bend up to 120° and the resonance frequency is 20 Hz.

2.2 Modeling and experimental characterization of pneumatic servovalves

During an electro-pneumatic control, the follow up of the power transfer from the source to the actuator is achieved through one or several openings with varying cross-section called restrictions: this monitoring organ is the servovalve [29]. The COLOBOT device is provided by three jet pipe micro-servovalves Atchley 200PN [30], which allow the desired modulation of air inside the different active chambers in Fig. 3(b). In this component, a motor is connected to an oscillating nozzle, which deflects the gas stream to one of

the two cylinder chambers (Fig. 4(a)). A voltage/current amplifier allows to control the servovalves by the voltage [31]. A first pneumatic output of this component is directly connected to one of the robot chambers, and a second output is left unconnected. A sensor pressure (UCC model PDT010131) (Fig. 4(b)) is used to measure the pressure in each of the three COLOBOT robot chambers. The measured pressure, comprised between 0 and 10 bars, was used to determine the servovalve control voltage.

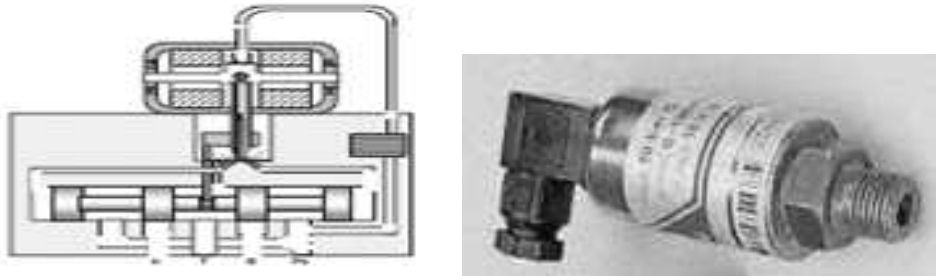

(a) Atchley servovalve 200PN (b) Pressure sensor

Fig. 4. Atchley servovalve and pressure sensor

As the three servo valves used for the COLOBOT actuator are identical, a random servovalve was chosen for the mass flow and pressure characterization. The pressure gain curve is the relationship between the pressure and the current control when the mass flow rate is null. It is performed by means of the pneumatic test bench shown in Fig 5. A manometer was placed downstream of the servovalve close by the utilization orifice in order to measure the pressures. Fig. 6 shows the pressure measurements P_n and P_p carried out for an increasing and a decreasing input current. It appears that the behavior of the servovalve is quite symmetric but with a hysteresis cycle. Arrival in stop frame couple creates pressure saturation at -18 mA, respectively +18 mA, for the negative current, respectively for the positive current. In the Fig. 5, we substitute the manometer on the test bench for a static mass flow-meter to plot the mass flow rate gain curve (mass flow rate with respect to the input current). This curve presented in Fig. 7 shows a non linear hysteresis.

Because of the specific size of Colobot's chambers, the experimental mass flow rate inside the the chamber is very small, the current input and the pressure variations are small enough to neglect the hysteresis and consider linear characteristics for Fig. 6 and Fig. 7.

2.3 Optical Fibre proximity sensors

The purpose of this robotic system is to guide the insertion of the colonoscope through the colon. So it is necessary to integrate the sensors to detect the position of the tip inside the colon. Due to the specific operation environments

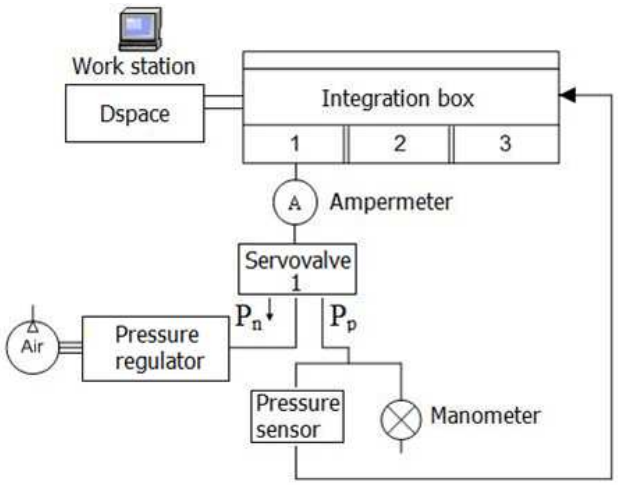

Fig. 5. Pressure gain pneumatic characterization bench

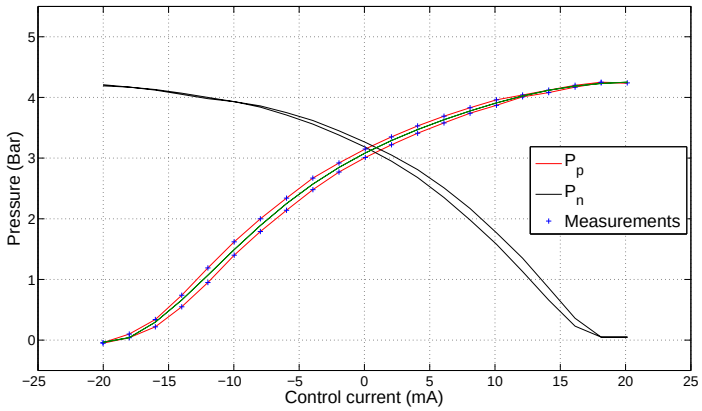

Fig. 6. Pressure gain characterization

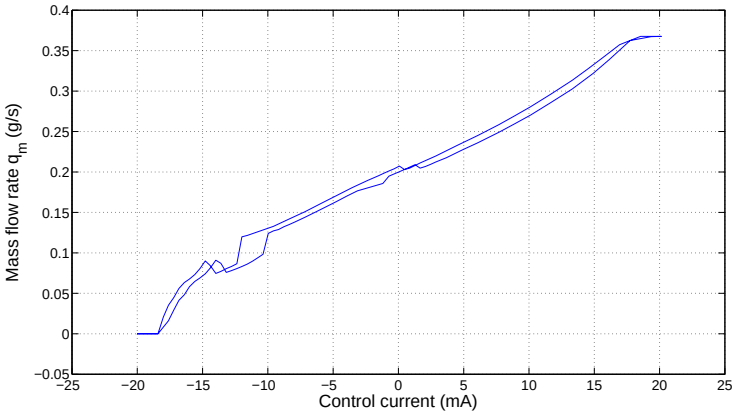

Fig. 7. Mass flow gain characterization

and the small space constraint, two important criteria must be taken into account to choose the distance sensors:

- the flexibility and size of the colonoscope,
- the cleanliness of the colon wall.

Tests have been performed using ultrasound and magnetic sensors as well as optical fibre. We decided to use optical fibre because of its flexibility, small size, high resolution, and the possibility of reflecting light off the porcine intestinal wall [16].This optical fibre system consists of one emission fibre and a group of four reception fibres (Fig. 8(a)). The light is emitted from a cold light source and conveyed by transmission fibres. After reflection on an unspecified body in front of the emission fibre, the reception fibres surrounding the emission fibre detect the reflected light. The amount of reflected light detected is a function of the distance between the sensor and the body. Figure 8(b) shows the output voltage determined by the distance between the sensor and the porcine intestinal wall. This curve shows that the sensor's resolution is sufficient for detecting the intestinal wall up to 8 mm. Fig. 9 shows the Colobot integrated three fibre optic proximity sensors. The first optical fibre is placed in front of the first pneumatic chamber and the other two in front of their individual pneumatic chambers.

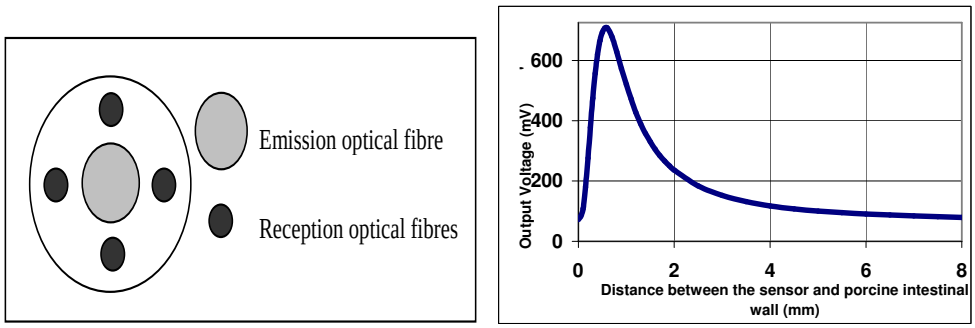

(a) Cross section of the optical fibre proximity sensor

(b) Characteristic of the optical fibre sensors

Fig. 8. Proximity sensors and its characterisation

3 Kinematic modeling the tip and the proximity sensor system

This section will deal with the kinematic modeling of the robotic tip and the model of the optical fibre sensors.

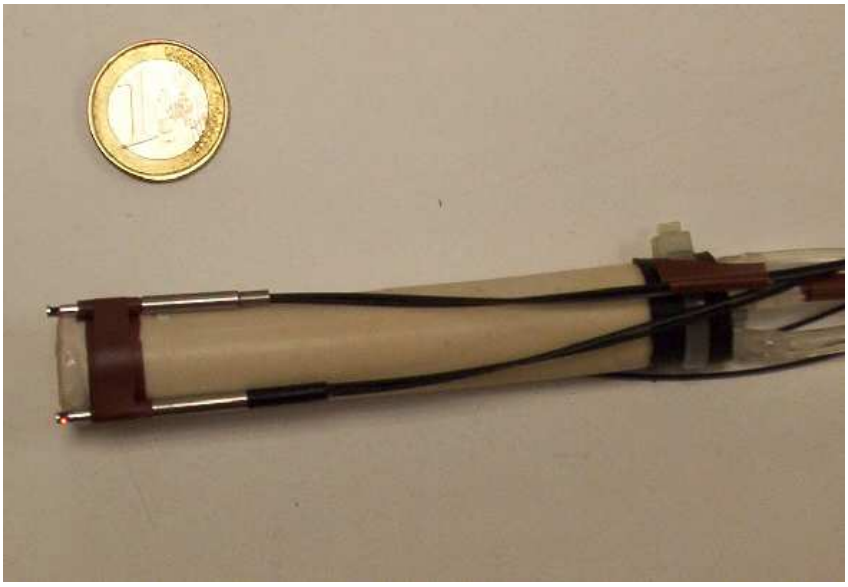

Fig. 9. Prototype integrated with optical fibre proximity sensors

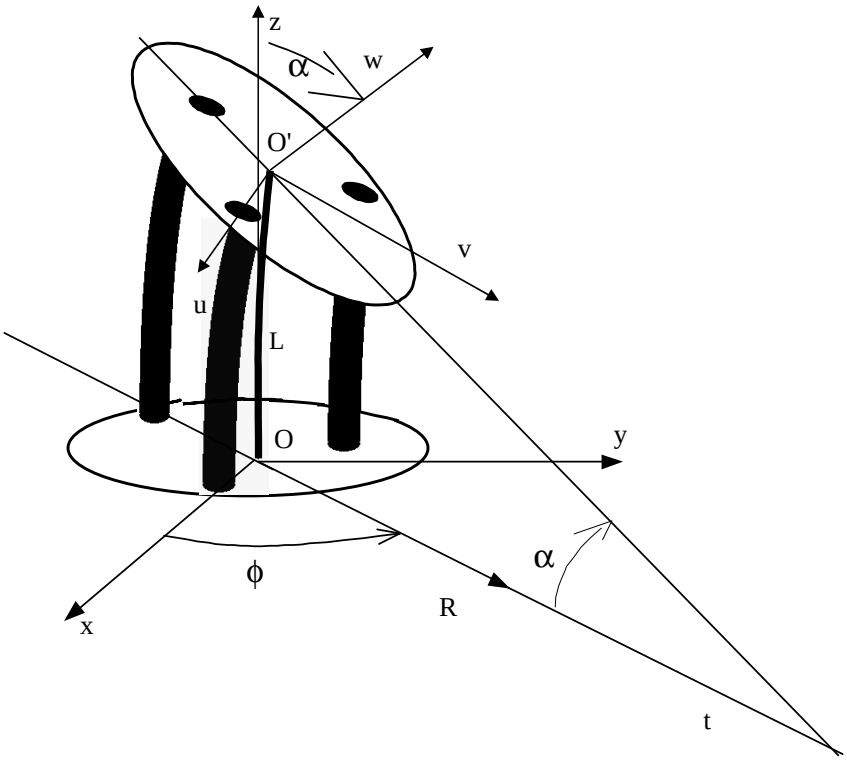

Fig. 10. Kinematic parameters of Colobot

3.1 Kinematic analysis of the robotic tip

Fig. 10 shows the robot shape parameters and the corresponding frames. The deformation shape of ColoBot is characterized by three parameters as done in our previous prototype EDORA [32]. It is worth to note that [2,24,26,28,33,34]

used almost the same set of parameters for the modeling:

- L is the length of the virtual center line of the robotic tip
- α is the bending angle in the bending plane
- ϕ is the orientation of the bending plane

The frame R_u (O-xyz) is fixed at the base of the actuator. The X-axis is the one that passed by the center of the bottom end and the center of the chamber 1. The XY-plane defines the plane of the bottom of the actuator, and the z-axis is orthogonal to this plane. The frame R_s (u, v, w) is attached to the top end of the manipulator. So the bending angle α is defined as the angle between the o-z axis and o-w axis. The orientation angle ϕ is defined as the angle between the o-x axis and o-t axis, where o-t axis is the project of o-w axis on the plan x-o-y. Given the assumption that the shape at the bending moment is an arc of a circle, the geometry-based kinematic model [32] relating the robot shape parameters to the actuator inputs (chamber length) is expressed as follows:

$$\begin{cases} L = \dfrac{1}{3}\displaystyle\sum_{i=1}^{3} L_i \\ \phi = \text{atan2}\dfrac{\sqrt{3}(L_2 - L_3)}{L_3 + L_2 - 2L_1} \\ \alpha = \dfrac{2\sqrt{\lambda_L}}{3r} \end{cases} \tag{1}$$

where $\lambda_L = {L_1}^2 + {L_2}^2 + {L_3}^2 - L_1L_2 - L_2L_3 - L_3L_1$ and r is the radius of the Colobot. And the direct kinematic equations with respect to the input pressures are represented by:

$$\begin{cases} L = L_0 + \dfrac{1}{3}\displaystyle\sum_{I=1}^{3} f_i(P_i) \\ \phi = \text{atan2}\dfrac{\sqrt{3}(f_2(P_2) - f_3(P_3))}{f_3(P_3) + f_2(P_2) - 2f_1(P_1)} \\ \alpha = \dfrac{\sqrt{\lambda_p}}{h} \end{cases} \tag{2}$$

where:

$$\lambda_p = f_1(P_1)^2 + f_2(P_2)^2 + f_3(P_3)^2 - f_1(P_1)f_2(P_2) - f_2(P_2)f_3(P_3) - f_3(P_3)f_1(P_1)$$

The function $f_i(P_i)$ $(i = 1, 2, 3)$ shows the relationship relating the stretch length of the chamber to the pressure variation of the silicone-based actuator as described as:

$$\Delta L_i = f_i(P_i) \tag{3}$$

Where ΔL_i $(i = 1, 2, 3)$ is the stretch length of each chamber with corresponding pressure and f_i $(i = 1, 2, 3)$ is a nonlinear function of P_i. The corresponding

results can be written as:

$$\begin{cases} \text{if} \quad P_{1min} < P_1 < P_{1max} \\ \Delta L_1 = 37(P_1 - P_{1min})^3 - 54(P_1 - P_{1min})^2 \\ \qquad -9.5(P_1 - P_{1min}) \\ \text{if} \quad P_{2min} < P_2 < P_{2max} \\ \Delta L_2 = -9(P_2 - P_{2min})^3 - 18(P_2 - P_{2min})^2 \\ \qquad -11(P_2 - P_{2min}) \\ \text{if} \quad P_{3min} < P_3 < P_{3max} \\ \Delta L_3 = 0.8(P_3 - P_{3min})^3 - 8.9(P_3 - P_{3min})^2 \\ \qquad -34(P_3 - P_{3min}) \end{cases} \tag{4}$$

where P_{imin} $(i = 1, 2, 3)$ is the threshold of the working point of each chamber and their values equal: $P_{1min} = 0.7\ bar$, $P_{2min} = 0.8\ bar$, $P_{3min} = 0.8\ bar$ and P_{imax} $(i = 1, 2, 3)$ is the maximum pressure that can be applied into each chamber. The detailed deduction of these equations can be found in [32].
The Cartesian coordinates (x, y, z) of the distal end of Colobot in the task space related to the robot bending parameters is obtained through a cylindrical coordinate transformation:

$$\begin{cases} x = \dfrac{L}{\alpha}(1 - \cos\alpha)\cos\phi \\ y = \dfrac{L}{\alpha}(1 - \cos\alpha)\sin\phi \\ z = \dfrac{L}{\alpha}\sin\alpha \end{cases} \tag{5}$$

And the state-space form of this model is given by:

$$X = f(Q_p) \tag{6}$$

where $X = (\alpha, \phi, L)^T, Q_p = (P_1, P_2, P_3)^T$.

3.2 Modeling and calibration of optical fibre sensors

For the preliminary test of our system, a transparent tube will be used which will be detailed in section6. So the distance model of the optical fibre sensors with respect to this tube needs to obtained before performing the test. Experimental methods are uses to obtain the model of each sensor. The voltage (u_i in volts) with respect to the distance (d_i in mm) between the sensor and the

tube wall is measured. Fig. 11 shows the measurements and the approximation model of the third sensor. The model of each sensor is obtained as follows:

$$u_1 = \frac{-40}{3.2d_1^2 + 3} \tag{7}$$

$$u_2 = \frac{-50}{1.6d_2^2 + 2.2} \tag{8}$$

$$u_3 = \frac{-38}{1.7d_3^2 + 2.3} \tag{9}$$

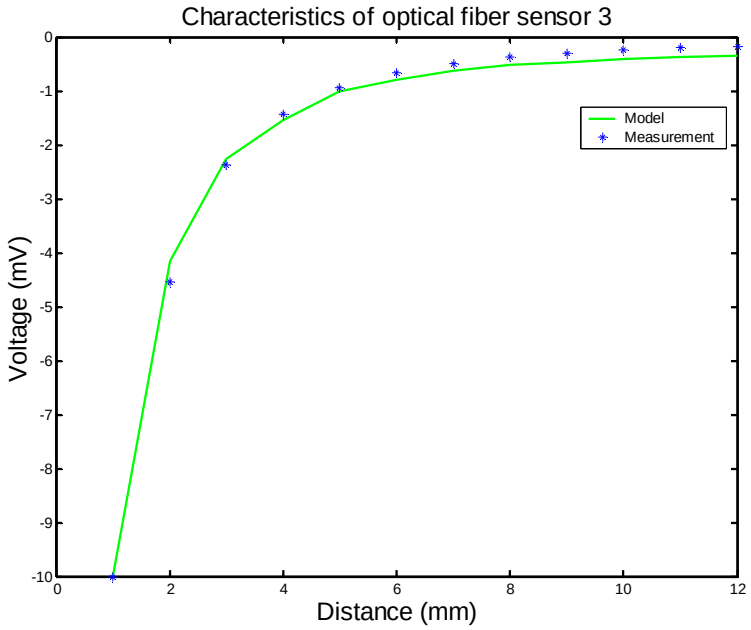

Fig. 11. modeling of optical fiber sensor

4 Validation of the kinematic model

Since the kinematics of Colobot has been described as the relationship between the deflected shape and the lengths of the three chambers (three pressures of each chamber), the validation of the kinematic model needs to have a sensor to measure the deflected shape, *i.e.* the bending angle, the arc length and the orientation angle. This section first presents sensor choice and its experimental setup for determining these system parameters, and presents the validation of the static kinematic model.

4.1 The sensor choice and experimental setup

For most continuum style robots, the determination of the manipulator shape is a big problem because of the dimension and the inability to mount measurement device for the joint angles. Although there are several technologies that could solve this problem for large size robots [33], they are difficult to implement on a micro-robot. Since a Cartesian frame has been analyzed with relation to the deflected shape parameters, an indirect method is used to validate the kinematic model with the 3D position measurement. For this purpose, an electromagnetic miniBIRD sensor is used for the experimental validation.

MiniBIRD is a six degree-of-freedom (position and orientation) measuring device from Ascension Technology Corporation [35]. It consists of one or more Ascension Bird electronic units, a transmitter and one or more sensors, see Fig.12. It offers full functionality of other magnetic trackers, with miniaturized sensors as small as 5mm wide. For data acquisition, the bottom of Colobot

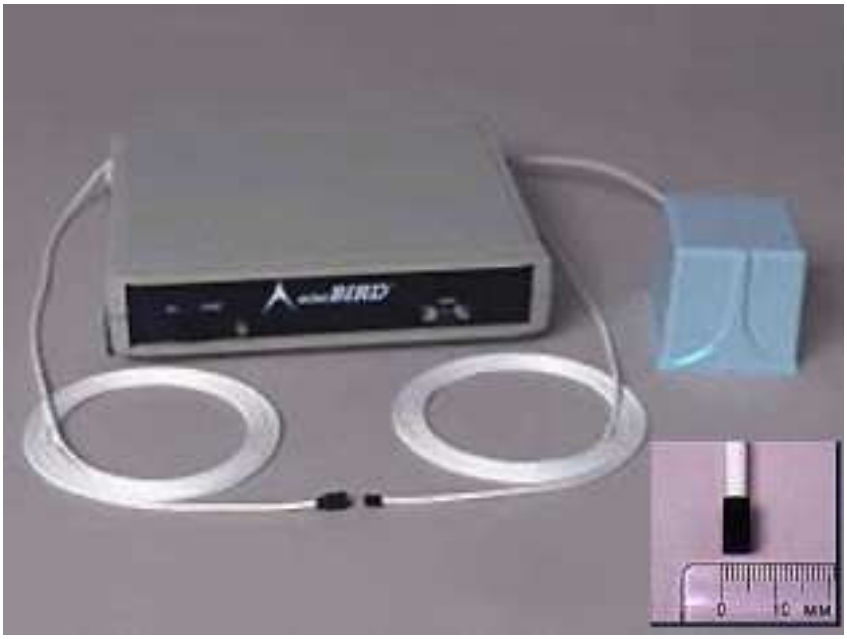

Fig. 12. MiniBIRD 6 DOF magnetic sensor

is bounded to a fixture and the sensor is placed on the top of Colobot, shown in Fig. 12. The transmitter is placed at a stationary position. Thus the position and orientation of top-end of Colobot are directly measured from the sensor receiver- with relation to the transmitter, and then the position of top-end of the manipulator with relation to the bottom of the manipulator is calculated indirectly through reference transformation.

Fig. 13. Measurement configuration

4.2 Validation of the static model

Using the sensor configuration, an open-loop experiment was carried out to validate the static model of the bending angle and the orientation angle (Eq. 2). As for the validation of bending angle, one orientation of Colobot movement is used for validation. The bending angle is directly measured from the miniBIRD sensor and compared with theoretical results from actual pressure obtained from the proportional valves. As shown in Fig. 14, the bending angle concerning the chamber length and the chamber pressure respectively has almost the same characteristics compared with the actual measurements.

To check the orientation angle, the position in the XY frame coordinate of the top-end of Colobot are measured for the six principal directions of the manipulator. Firstly, expected pressure combinations were used for Colobot to follow the six principal orientation angles $(0°, 60°, 120°, 180°, 240°, 300°)$ while the bending angle varied from $0°$ to the maximum. Then the measured positions of the top-end of Colobot were plotted relative to the original position of Colobot without deformation. This experimental protocol leads to Fig. 15. This figure highlights that the six orientation angles are in accordance with the theoretical values except for high pressures in the chambers.

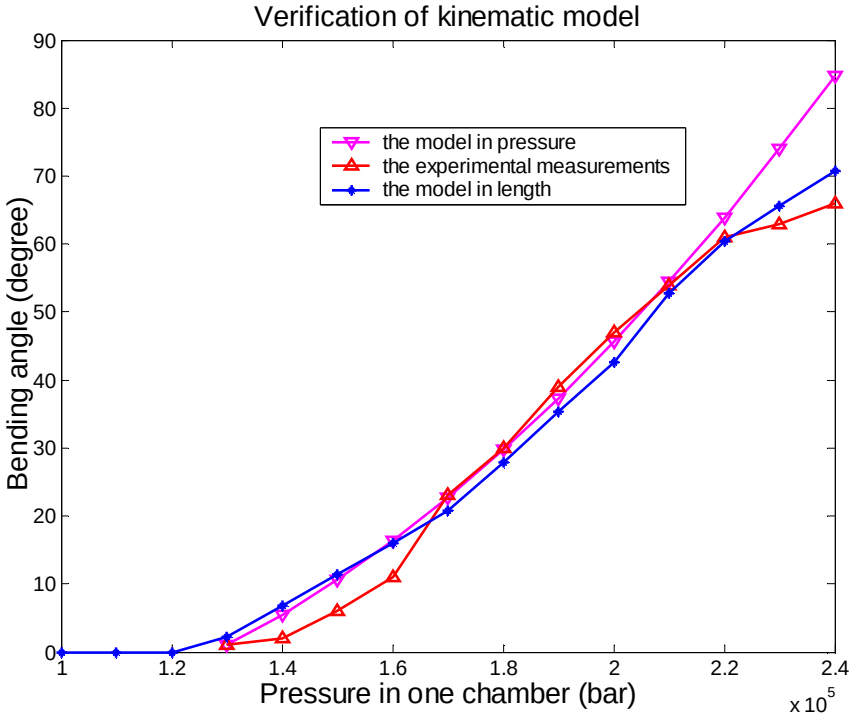

Fig. 14. Comparisons of the bending angle with relation to the chamber length and chamber pressure

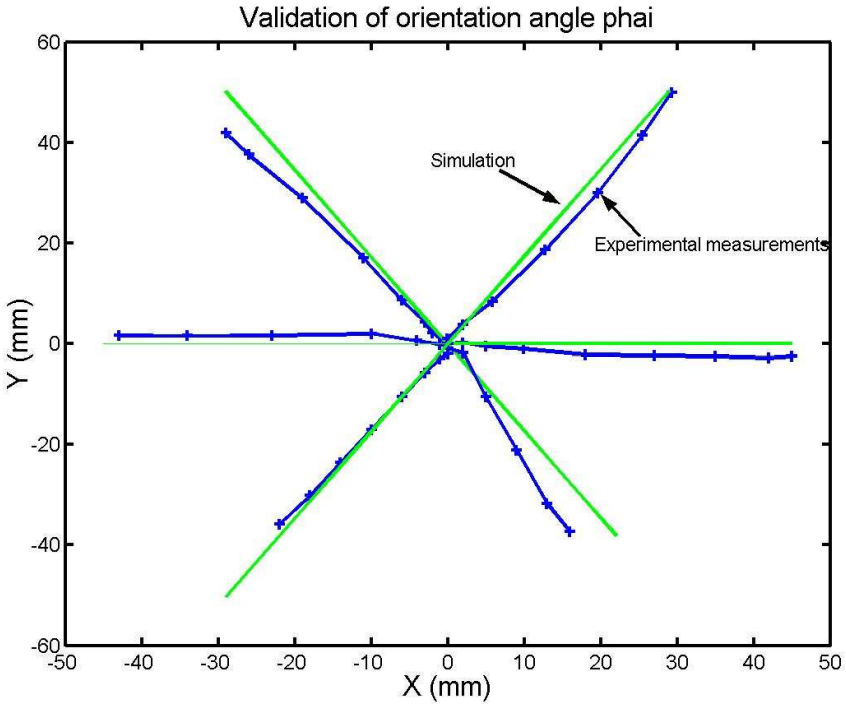

Fig. 15. Comparison of the orientation angle: measurement and simulation

Section 4.2 validated the bending angle and orientation angle separately in static. However, most of the time the motion of the device results from the pressure differentials between each chamber, this is to say, the interaction of each chamber. So it is necessary to check this mutual interaction between each chamber. To achieve this goal, sinus reference signals of pressure with 120° delay are applied to each servovalve. They are employed to make Colobot turn around its vertical axis with a constant velocity (see the experimental setup Fig. 13) to see the mutual interaction of each chamber. By using miniBIRD, the endpoint coordinates of Colobot can be obtained in XOY plane. Thus the comparison between these coordinates and those obtained from the simulation of the kinematic model (Eq. 5) allows us to check if there are interactions of each chamber on the elongation of the prototype.

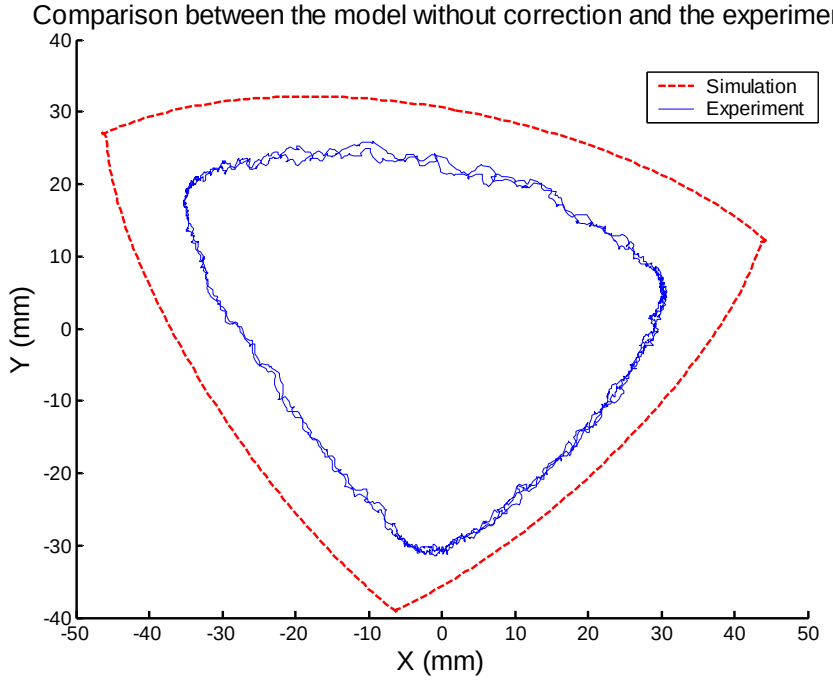

Fig. 16. Simulation et experimental results of the movement of the Colobot's tip (across dead zone)

Two comparisons are then proposed in Figures 16 and 17. For the first case, three sinus signals of pressure with amplitude of 0.4 bar and an offset of 0.9 bar are applied in the chambers of the prototype. The path of the endpoint of Colobot is a form of triangle (Fig. 16) because these actuators of Colobot work across the threshold of their dead zones. For the latter case, three sinus signals of pressure with amplitude of 0.4 bar and an offset of 1.2 bar are applied in the chamber of Colobot. In this case, Colobot works in the working zone and the endpoint path of Colobot lead to a circular shape (Fig. 17). The lines in

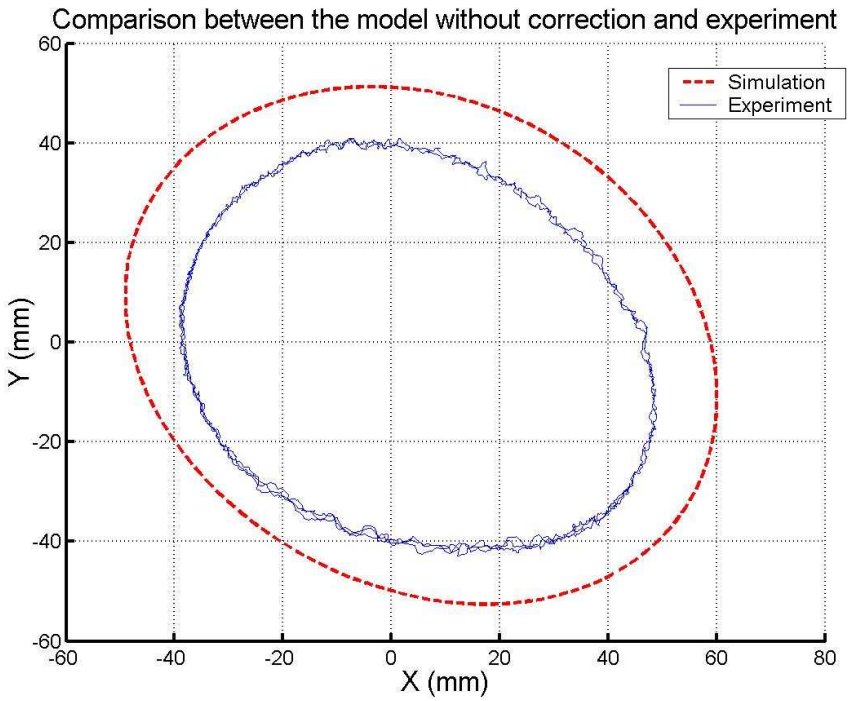

Fig. 17. Simulation and experimental results of the movement of the endpoint of Colobot

the outer layer are the simulation result from the kinematic model relating XY coordinates to the corresponding pressure of each chamber (Eq. 4). Since the characteristics of deformation under pressure is performed each chamber by each chamber independently (Eq. 4), the difference between the results of simulation and the experimental results showed in Figure 16 and Figure 17 suggests that there exist interactions among each chamber. This interaction is taken into account in section 4.4.

4.4 Estimation of a correction parameter

In this section, new parameters are chosen to represent the interactions between each chamber. Thus, six stiffness parameters are introduced to describe the coupling effect of stretching of one chamber to that of other two chambers. Let denotes k_{ij} the mutual stiffness that determines the effect of P_i (i=1,2,3) on the length of the chamber j (j = 1,2,3) (where i does not equal j). The coefficients are obtained by minimizing the difference between the operational coordinates (X_s, Y_s) measured by miniBIRD and the operational coordinates (X_m, Y_m) obtained by simulation of the kinematic model (Fig. 18).

A classical non-linear optimization based on the Levenberg-Marquardt algorithm is proceeded to adjust the unknown parameters k_{ij}. The cost criterion

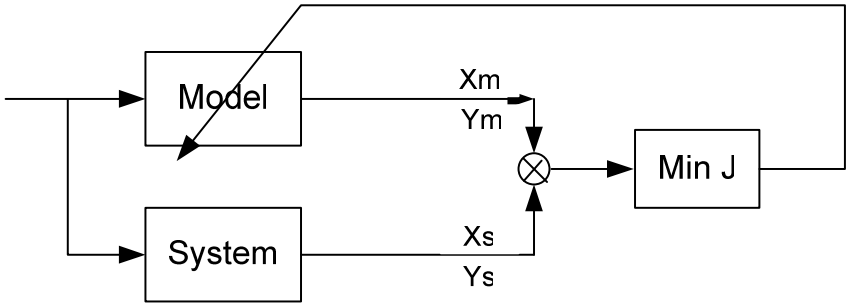

Fig. 18. Optimization model

chosen is:

$$J(k_{ij}) = \left\| \sqrt{(X_s)^2 + (Y_s)^2} - \sqrt{k_{ij}(X_m)^2 + k_{ij}(Y_m)^2)} \right\| \tag{10}$$

The numerical results roughly lead to the same coefficient $k = 0.3$ for the unknown parameters k_{ij}. Thus the new expression of the kinematic model is given by:

$$\begin{cases} \Delta L_1 = f_1(P_1) + 0.3(f_2(P_2) + f_3(P_3)) \\ \Delta L_2 = f_2(P_2) + 0.3(f_1(P_1) + f_3(P_3)) \\ \Delta L_3 = f_3(P_3) + 0.3(f_1(P_1) + f_2(P_2)) \end{cases} \tag{11}$$

It is noteworthy that the elongation expression ΔL_1 (respectively ΔL_2, ΔL_3) in (Eq. 11) is equivalent to (Eq. 3) when the relative pressures P_2 and P_3 (respectively P_1, P_3 and P_1, P_2) are equal to zero.

To check this new kinematic model a cross validation is made with three other experiments. Three sinus input pressures with amplitude from 0.1 bar to 0.3 bar are applied into three chambers of Colobot. The improved kinematic model with the correction coefficient k is used to a straightforward comparison with the sets of data. Results shown in Fig. 19 and Fig. 20 are testimony to the behavior of the proposed model in these two cases.

5 Guidance control strategy based on proximity multi-sensor system

5.1 Guidance control strategy

The objective of sensor-based guidance strategy is to calculate the safe position of the distal-end of Colobot compared to the colon wall in real-time based on the measurements of three distance sensors for guidance inside the colon. For the sake of simplicity but without loss of generality, it is assumed that a colon

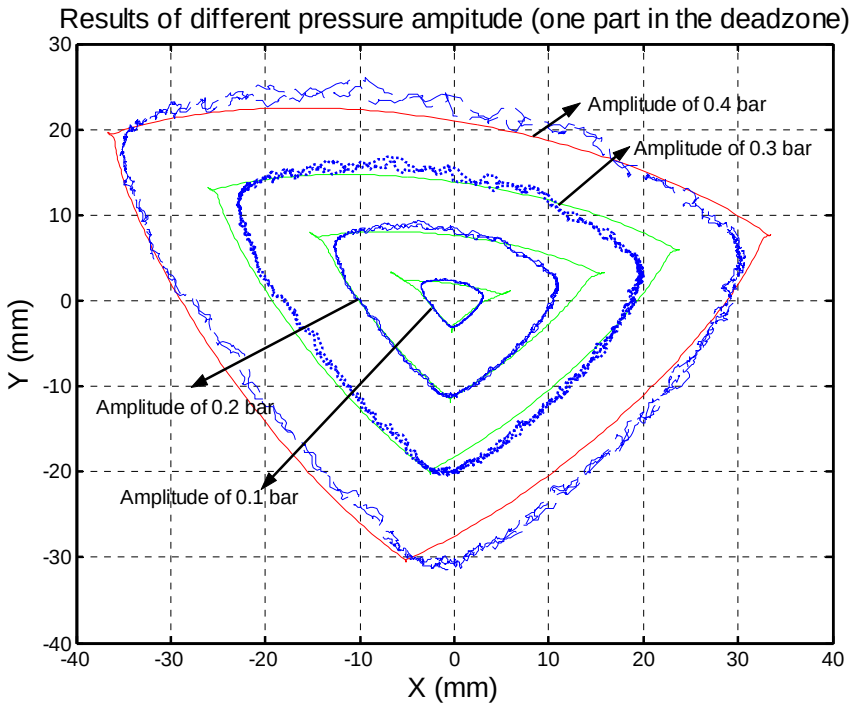

Fig. 19. Verification of corrected with different pressure inputs (across dead zone)

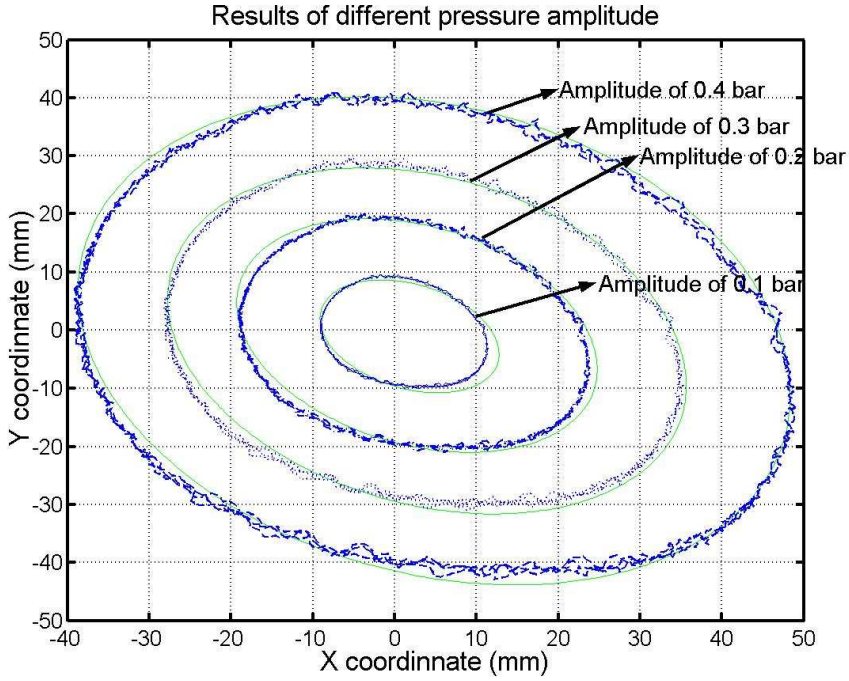

Fig. 20. Validation with different pressure inputs

is a cylindrical tube and its cross section is an ellipse at the sensor plane. Fig. 21 illustrates the sensor plane, the distal end of ColoBot and the colon axis. With these assumptions, the safe position will be the central axis of the colon. To approximate the colon axis, a method based on a circumscribed circle is proposed. Since three points D_1, D_2 and D_3 (Fig. 22) of sensor measurements

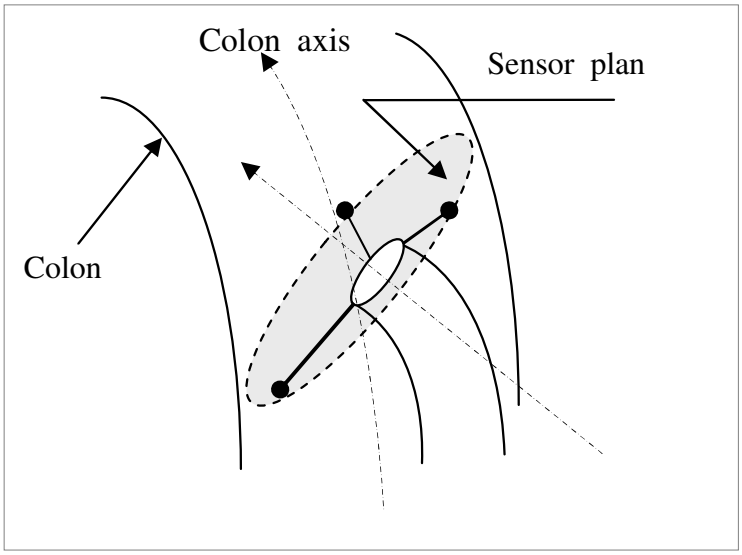

Fig. 21. Position of Colobot inside the colon

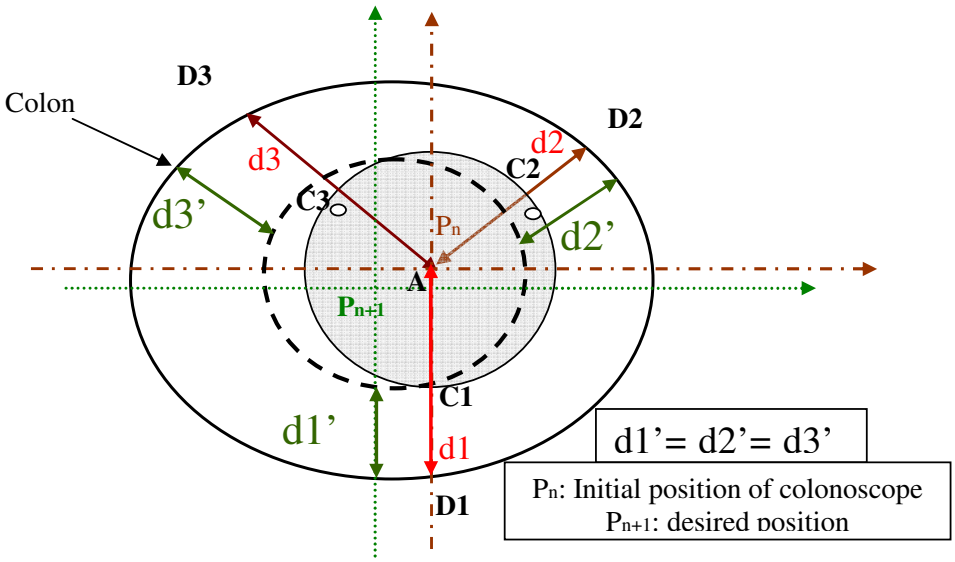

Fig. 22. Computation of the safe position

form a triangle, the center of the circumscribed circle of this triangle is chosen as the safe position. This approach iterates as following:

- Three sensor measurements are collected.
- Position P_n in the frame R_s (Fig. 22) is evaluated with these three measurements.
- If P_n is a safe position, then it's necessary to go back to the first step for the next period; otherwise, next the safe position P_{n+1} described in the Frame R_u (Fig. 22) is calculated through the circumscribed method and is provided to the kinematic control for execution.

For more details about the guidance control strategy, please find the reference [36].

5.2 Guidance control architecture

The control of Colobot is organized in three hierarchical levels, as shown in Fig. 23. The first level consists of local pressure control of each chamber of the Colobot through three servovalves. Three independent PI controllers are used to implement the closed-loop pressure control of the chamber. The position and orientation of Colobot are controlled at level 2 using an instantaneous inverse Jacobian method. This section will describe the implementation detail. Level 3 is the sensor-based planning for automatic navigation described in section 5.1.

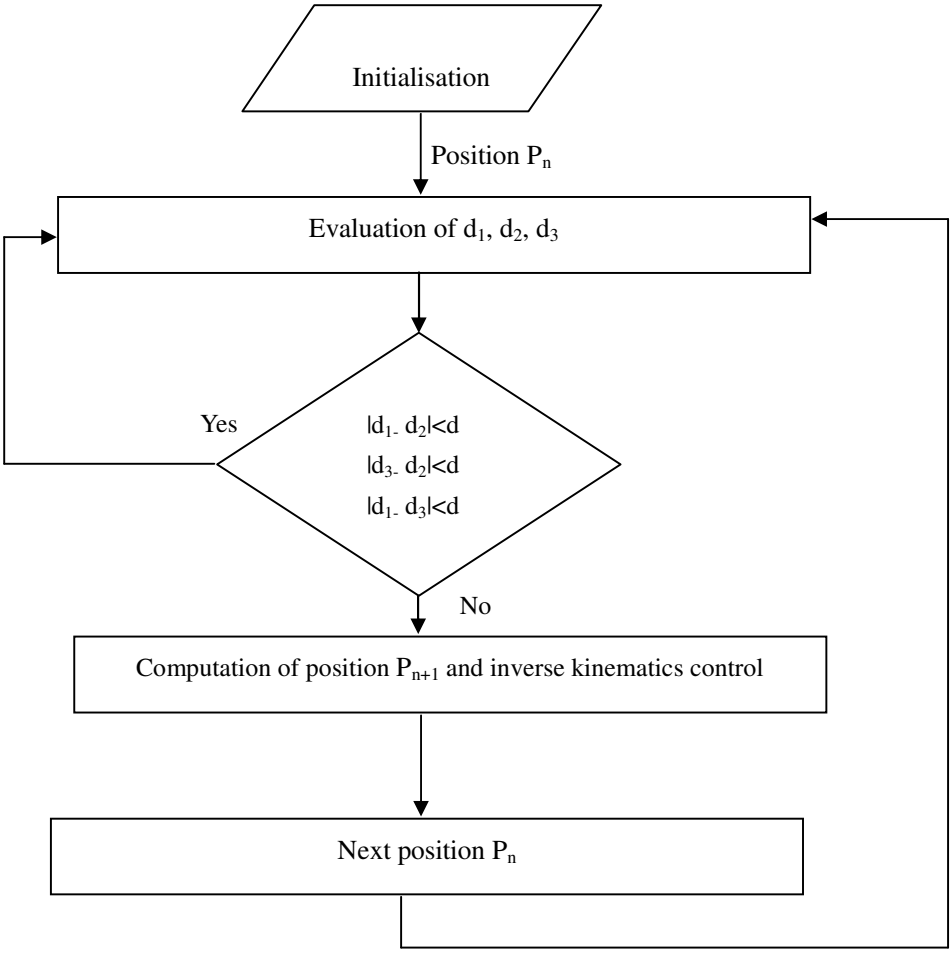

Fig. 23. sensor-based planning and guidance control procedure

5.3 Formulation of task space control of Colobot

After determining the desired trajectory from sensor-based planning, the kinematic control of Colobot will be described in this section. It should be noted that two variables are used to represent the position of Colobot inside the colon. However, the Colobot has 3 degrees of freedom. So this manipulator becomes redundant for the chosen task. The velocity kinematic equations are rewritten as following:

$$\begin{aligned} X &= f(Q_p) \\ \dot{X} &= \frac{\partial X}{\partial(\alpha,\phi,L)} \frac{\partial(\alpha,\phi,L)}{\partial Q_L}\frac{\partial Q_L}{\partial Q_P}\dot{Q}_p \quad \text{or} \\ \dot{X} &= J_s J_l J_p \dot{Q}_p = J\dot{Q}_p \end{aligned} \tag{12}$$

where $X = (x, y)^T, Q_L = (L_1, L_2, L_3)^T, Q_p = (P_1, P_2, P_3)^T$ and $J = J_s J_l J_p$ is the Jacobian matrix with relation to the three levels of pressure in the chambers.

5.4 Resolution of the inverse kinematics with redundancy

In the case of a redundant manipulator with respect to a given task, the inverse kinematic problem admits infinite solutions. This suggests that redundancy can be conveniently exploited to meet additional constraints on the kinematic control problem in order to obtain greater manipulability in terms of the manipulator configurations and interaction with the environment. A viable solution method is to formulate the problem as a constrained linear optimization problem. Work on resolved-rate control [37] proposed to use the Moore-Penrose pseudo inversion of the Jacobian matrix as:

$$\dot{Q}_p = J^+\dot{X} = (J^T(JJ^T)^{-1})\dot{X} \tag{13}$$

In our case, however, there is a mechanical limit range for the elongation of each chamber and the corresponding pressure applied into the chamber of the Colobot. The objective function is constructed to be included in the inverse Jacobian algorithms as the second criteria also called the null-space method [38,39].

$$\dot{Q}_p = J^+\dot{X} + \mu[I - J^+J]\dot{g} \tag{14}$$

where I is the identity matrix, μ is constant and g is a second criterion for the optimization of the solution. This objective function evaluates the pressure difference between the applied pressure in the chamber and the average pressure applied in the chamber. So the cost function $w(P)$ is expressed as

follows:

$$w(P) = \frac{1}{3}\sum_{i=1}^{3}\left(\frac{P_i - P_{iave}}{P_{imax} - P_{imin}}\right)^2 \tag{15}$$

We can then minimize $w(p)$ by choosing:

$$\dot{g} = \mathrm{grad}\,(w(P)) = \left\{ \frac{\partial w}{\partial P_1}\frac{\partial w}{\partial P_2}\frac{\partial w}{\partial P_3} \right\} \tag{16}$$

6 Experimental results

This section will present the implementation of the whole system and experimental results of automatic guidance capability of this system in a colon-like tube.

6.1 Hardware implementation

Fig. 24 shows the low-level control system of ColoBot. The pressurized air comes through the compressor (1) and the general pressure is adjusted thanks to the device (2). The pressure in the chambers are controlled by three Jet-pipe servovalves (3a, 3b and 3c). Three pressure sensors (4a, 4b and 4c) are connected between the servovalves and the Colobot (5) for the pressure feedback control. Suitable drivers and amplifiers in the rack (6) were designed to amplify control signals applied to the actuator. A real-time controller is implemented through a DSpace board and coupled with the Real-Time Workshop of Simulink. The Simulink block diagram designed for path planning and kinematics algorithms are expressed with Simulink block diagram which will be compiled as real-time executable under the DSP Processor of the DSpace board. The system runs at 500 Hz for a real-time control loop.

6.2 Experimental results in a colon-like tube

A more realistic experiment to test the performance of this semi-autonomous colonoscopy system is to use a colon-like transparent tube to see if Colobot can cross the tube with minimal contact with the tube wall. The diameter of the tube is 26 mm and its length is 50 cm (Fig. 25). For this guidance experiment, the calibration of the optical fibres was adapted to the transparent tube. It is highly probable that results for the distance sensors in a porcine intestine will be similar to those obtained in the human bowel. However, the locomotion of the system is manually operated. The evolution of the measurements of three

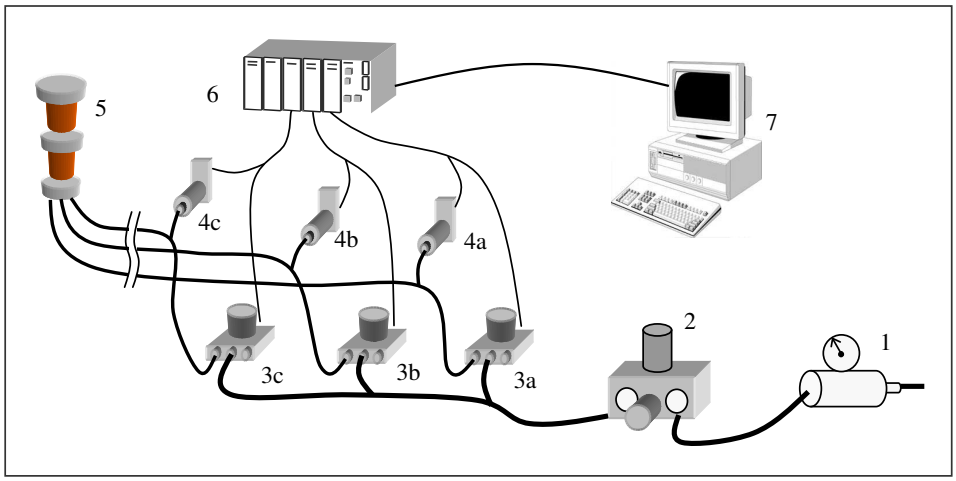

Fig. 24. The implementation of the whole system

optical fibres are represented in the left Fig. 26(a). During the entire movement, the distances are never less than 0.8 mm. This demonstrates that the colonoscope tip is moving through the tube without touching it. For a better representation and visualization, Fig. 26(b) shows the extreme positions of the top-end of Colobot as it progresses (with a velocity of 4 cm/s). The position of the Colobot at the centre of the tube is represented by the smallest circle. The larger circle represents the tube wall and the line shows the extreme positions of Colobot. This experiment demonstrates that Colobot has the capability to guide the exploration of the tube with a sensor-based steering control method.

Fig. 25. Guidance control test in a colon-like tube

7 CONCLUSIONS AND FUTURE WORKS

This paper presented a complete robotic system for semi-autonomous colonoscopy. It is composed of a microtip, a proximity multi-sensor system and high level real-time control system for guidance control of this robot. This system was focused on its guidance ability of endoscope inside the human colon with the

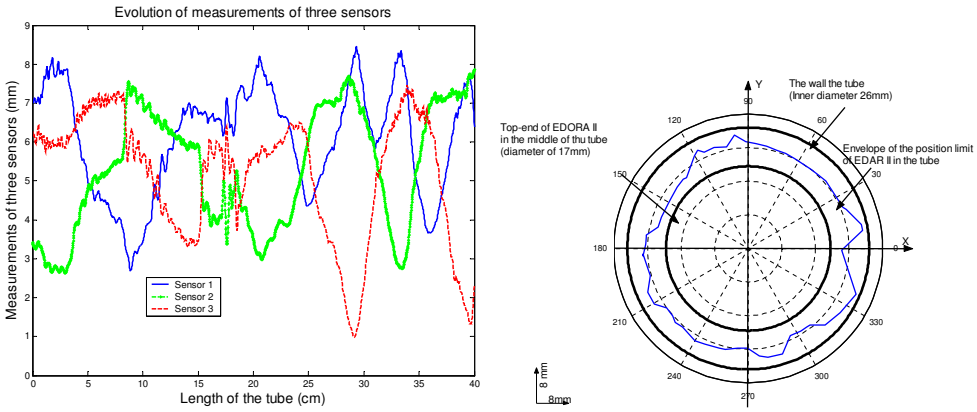

(a) Evolution of three measurements (b) Extreme position projected into the tube plane

Fig. 26. Guidance control result analysis

fiber optic proximity sensors. Colobot is a continuum robot made of silicone rubber. It has three DoF with its outer diameter of 17mm and the weight of 20 gram. The pneumatic actuators of ColoBot are independently driven through three servovalves. The kinematic model of this soft robot was developed based on the geometric deformation and validated its correction. A method based on a circumscribed circle is utilized to calculate the safe reference position and orientation of the Colobot. While kinematic-based orientation control used these reference paths to adjust the position of Colobot inside the colon to achieve guidance. Experimental results of guidance control with a transparent tube verified the effectivity of kinematic control and guidance control strategy. In the near future, the proposed method will be tested in a vitro environment.

References

[1] R. H. Taylor, D. Stoianovici, Medical robotics in computer-integrated surgery, IEEE Transaction on Robotics and Automation 19 (5) (2003) 765–781.

[2] N. Simaan, R. Taylor, P. Flint, A dexterous system for laryngeal surgery- multi-backbone bending snake-like slaves for teleoperated dexterous surgical tool manipulation, in: IEEE International Conference on Robotics and Automation, New Orleans, USA, 2004, pp. 351–357.

[3] R. J. I. Webster, J. M. Romano, N. J. Cowan, Mechanics of precurved-tube continuum robots, IEEE Transactions on Robotics 25 (1) (2009) 67 – 78.

[4] D. P. C. M.C., P. A., Development and in vitro tests of a miniature robotic system for computer-assisted colonoscopy, Jounal of Computer Aided Surgery, 4 (1999) 4–14.

[5] R. H. Sturges, A flexible, tendon-controlled device for endoscopy, The International Journal of Robotics Research 12 (2) (1993) 121–131.

[6] T. Fukuda, S. Guo, K. Kosuge, F. Arai, M. Negoro, K. Nakabayashi, Micro active catheter system with multi degrees of freedom, in: Proceedings of the International Conference on Robotics and Automation, San Diego, USA, 1994, pp. 2290–2295.

[7] S. Phee, W. S. Ng, I.-M. Chen, F. Seow-choen, B. L. Davies, Automation of colonoscopy, part one: Locomotion and steering aspects in automation of colonoscopy, IEEE Engineering in Medecine and Biology Magazine 17 (3) (1998) 81–89.

[8] K. Ikuta, M. Tsukamoto, S. Hirose, Shape memory alloy servo actuator system with electric resistance feedback and application for active endoscope, in: IEEE International Conference on Robotics and Automation, Hitachi City, Japan, 1988, pp. 427–430.

[9] A. B. Slatkin, J. Burdick, The development of a robot endoscope, in: Proc. of the IEEE-RSJ Int. Conf. on Intelligent Robots and Systems, Pittsburgh, USA, 1995, pp. 3315–3320.

[10] P. Dario, C. Paggetti, N. Troisfontaine, E. Papa, T. Ciucci, M. Carrozza, M. Marcacci, A miniature steerable end-effector for application in an integrated system for computer-assisted arthroscopy, in: IEEE International Conference on Robotics and Automation, Albuquerque, USA, 1997, pp. 1573–1579.

[11] A. Menciassi, P. J.H., S. Lee, S. Gorini, P. Dario, J. Park, Robotic solutions and mechanisms for a semi-autonomous endoscope, in: Proc. of the IEEE-RSJ Int. Conf. on Intelligent Robots and Systems, Lausane, Switzerland, 2002, pp. 1379–1384.

[12] S. Kumar, I. Kassim, V. Asari, Design of a vision- guided microrobotic colonoscopy system, Advanced robotics 14 (2) (2000) 87–114.

[13] I. Kassim, W. Ng, G. Feng, S. Phee, Review of locomotion techniques for robotic colonoscopy, in: Proceedings of the International Conference on Robotics and Automation, Taipei, Taiwan, 2003, pp. 1086–1091.

[14] J. Piers, D. Reynaerts, H. Van Brussel, G. De Gersem, H. T. Tang, Design of an advanced tool guiding system for robotic surgery, in: Proceedings of the International Conference on Robotics and Automation, Taipei, Taiwan, 2003, pp. 2651–2656.

[15] B. Kim, H. Y. Lim, J. H. Par, J. Park, Inchworm-like colonoscopic robot with hollow body and steering device, JSME International Journal Series C 49 (1) (2006) 205–212.

[16] Tech. rep.
URL `http://www.rfnorika.com`

[17] Tech. rep.
URL `http://www.givenimaging.com`

[18] A. Menciassi, A. Moglia, S. Gorini, G. Pernorio, C. Stefnini, P. Dario, Shape memory alloy clamping devices of a capsule for monitoring tasks in the gastrointestinal tract, Journal of Micromechanics and Microengineering 15 (11) (2005) 2045–2055.

[19] M. Gorini, A. Menciassia, G. Pernorio, S. G., P. Dario, A novel sma-based actuator for a legged endoscopic capsule, in: IEEE/RAS-EMBS International Conference on Biomedical Robotics and Biomimetics, 2006.

[20] B. Kim, L. sunghak, P. J. Heong, P. Jong-oh, Design and fabrication of a locomotive mechanism for capsule-type endos using shape-memory alloys (sma), IEEE/ASME Transactions on Mechatronics 10 (1) (2005) 77–86.

[21] X. Wang, M. Q.-H. Meng, 2008 ieee/rsj international conference on intelligent robots and systems, Nice, France, 2008, pp. 1198–1203.

[22] P. Glass, E. Cheung, M. Sitti, A legged anchoring mechanism for capsule endoscopes using micropatterned adhesives, IEEE Transactions on Biomedical Engineering 55 (12) (2008) 2759–2767.

[23] G. Robinson, J. Davies, Continuum robots - a state of the art, in: IEEE International Conference on Robotics and Automation, Detroit Michigan, USA, 1999, pp. 2849–2853.

[24] D. Lane, J. David, G. Robinson, D. O'Brien, J. Sneddon, E. Seaton, E. A., The amadeus dextrous subsea hand: Design, modeling, and sensor processing, IEEE Journal of Oceanic engineering 24 (1) (1999) 96–111.

[25] G. Immega, K. Antonelli, The KSI tentacle manipulator, in: IEEE International Conference on Robotics and Automation, Nagoya, Japan, 1995, pp. 3149 –3154.

[26] Y. Bailly, Y. Amirat, Modeling and control of a hybrid continuum active catheter for aortic aneurysm treatment, in: IEEE International Conference on Robotics and Automation, Barcelona, Spain, 2005, pp. 924–929.

[27] G. Chen, M. T. Pham, T. Redarce, Development and kinematic analysis of a silicone-rubber bending tip for colonoscopy, in: IEEE/RSJ Intemational Conference on Intelligent Robots and Systems, Beijing, China, 2006, pp. 168–173.

[28] K. Suzumori, S. Iikura, H. Tannaka, Applying a flexible-micro-actuator robotic mechanisms, IEEE control systems 12 (1) (1992) 21–27.

[29] S. Sesmat, Modélisation, simulation et commande d'une servovalve electropneumatique (in french), Ph.D. thesis, INSA de Lyon (1996).

[30] Atchley Controls, Jet Pipe catalogue.

[31] R. Atchley, A more reliable electrohydraulic servovalve, in: Robot VI Conference, Detroit, USA, 1982.

[32] G. Chen, M. T. Pham, T. Redarce, C. Prelle, F. Lamarque, Design and control of an actuator for colonoscopy, in: 6th International Workshop on Research and Education in Mechatronic, Annecy, France, 2005, pp. 109–114.

[33] H. Ohno, S. Hirose, Design of slim slime robot and its gait of locomotion, in: Proc. of the IEEE-RSJ Int. Conf. on Intelligent Robots and Systems, Hawaii, USA, 2001, pp. 707–715.

[34] B. Jones, I. D. Walker, Kinematics for multi-section continuum robots, IEEE Transactions on Robotics 22 (1) (2006) 43 –55.

[35] Tech. rep.
URL http://www.ascension-tech.com/

[36] G. Chen, M. Pham, T. Redace, Sensor-based guidance control of a continuum robot for a semi-autonomous colonoscopy, Robotics and autonomous systems 57 (6) (2008) 712–722.

[37] D. Whitney, Resolved motion rate control of manipulators and human prostheses, IEEE Transaction on Man-Machine systems 10 (2) (1969) 47–53.

[38] J. Hollerbach, K. Suh, Redundancy resolution of manipulator through torque optimization, A.I.Memo 882, Massachussett Institute of Technology (1986).

[39] Y. Nakamura, Advanced robotics, Redundancy and Optimization, Addison-Wesley, 1991.